\



Nonlinear dynamics analysis of cluster-shaped conservative flows generated from a generalized thermostatted system

Yue Li(李月), Zengqiang Chen(陈增强), Zenghui Wang(王增会), and Shijian Cang(仓诗建)
Citation: Chin. Phys. B, 2022, 31 (**1**): 010501. DOI: 10.1088/1674-1056/ac0a61
Journal homepage: http://cpb.iphy.ac.cn; http://iopscience.iop.org/cpb

What follows is a list of articles you may be interested in

Dynamic modeling and aperiodically intermittent strategy for adaptive finite-time synchronization control of the multi-weighted complex transportation networks with multiple delays

Ning Li(李宁), Haiyi Sun(孙海义), Xin Jing(靖新), and Zhongtang Chen(陈仲堂)
Chin. Phys. B, 2021, 30 (**9**): 090507. DOI: 10.1088/1674-1056/abea92

Nonlinear vibration of iced cable under wind excitation using three-degree-of-freedom model

Wei Zhang(张伟), Ming-Yuan Li(李明远), Qi-Liang Wu(吴启亮), and An Xi(袭安)
Chin. Phys. B, 2021, 30 (**9**): 090503. DOI: 10.1088/1674-1056/abea83

Generating multi-layer nested chaotic attractor and its FPGA implementation

Xuenan Peng(彭雪楠), Yicheng Zeng(曾以成), Mengjiao Wang(王梦蛟), and Zhijun Li(李志军)
Chin. Phys. B, 2021, 30 (**6**): 060509. DOI: 10.1088/1674-1056/abda34

Complex network perspective on modelling chaotic systems via machine learning

Tong-Feng Weng(翁同峰), Xin-Xin Cao(曹欣欣), and Hui-Jie Yang(杨会杰)
Chin. Phys. B, 2021, 30 (**6**): 060506. DOI: 10.1088/1674-1056/abd9b3

Behaviors of thermalization for the Fermi-Pasta-Ulam-Tsingou system with small number of particles

Zhenjun Zhang(张振俊), Jing Kang(康静), and Wen Wen(文文)
Chin. Phys. B, 2021, 30 (**6**): 060505. DOI: 10.1088/1674-1056/abd92f

---

Nonlinear dynamics analysis of cluster-shaped conservative flows generated from a generalized thermostatted system

Yue Li(李月)[1], Zengqiang Chen(陈增强)[1], Zenghui Wang(王增会)[2], and Shijian Cang(仓诗建)[3,†]

[1] *College of Artificial Intelligence, Nankai University, Tianjin* 300350, *China*
[2] *Department of Electrical and Mining Engineering, University of South Africa, Florida* 1710, *South Africa*
[3] *Department of Product Design, Tianjin University of Science and Technology, Tianjin* 300222, *China*

(Received 13 April 2021; revised manuscript received 18 May 2021; accepted manuscript online 11 June 2021)

The thermostatted system is a conservative system different from Hamiltonian systems, and has attracted much attention because of its rich and different nonlinear dynamics. We report and analyze the multiple equilibria and curve axes of the cluster-shaped conservative flows generated from a generalized thermostatted system. It is found that the cluster-shaped structure is reflected in the geometry of the Hamiltonian, such as isosurfaces and local centers, and the shapes of cluster-shaped chaotic flows and invariant tori rely on the isosurfaces determined by initial conditions, while the numbers of clusters are subject to the local centers solved by the Hessian matrix of the Hamiltonian. Moreover, the study shows that the cluster-shaped chaotic flows and invariant tori are chained together by curve axes, which are the segments of equilibrium curves of the generalized thermostatted system. Furthermore, the interesting results are vividly demonstrated by the numerical simulations.

Keywords: multiple equilibria, curve axes, invariant tori, cluster-shaped conservative chaos

PACS: 05.45.–a **DOI:** 10.1088/1674-1056/ac0a61

1. Introduction

It is accepted that chaos generated from smooth and non-smooth nonlinear dynamical systems described by ordinary differential equations (ODEs) or partial differential equations (PDEs) can be divided into two categories: dissipative chaos (chaotic attractor) and conservative chaos (also known as Hamiltonian chaos). Dissipative chaos widely exists in physical systems, such as Chua's circuit,[1] double pendulum,[2] ballistic Dirac fermion systems,[3] the Peyrard–Bishop–Dauxois DNA model,[4] and some artificial nonlinear systems.[5–7] In contrast to dissipative chaos, conservative chaos can only be found in some theoretical models in the fields of celestial mechanics, molecular dynamics and hydrodynamics, such as the Hénon–Heiles system describing the motion of a star in a cylindrically symmetric and gravitationally smooth galactic potential,[8] two coupled anharmonic oscillators associated with molecular dynamics,[9] coupled Bloch oscillator equations representing electronic excitations of molecular dimers,[10] and hydrodynamic pilot-wave system.[11] So far, the existing results have shown that the conservative chaos can be generated by Hamiltonian systems[12,13] as well as thermostatted systems.[14–17] Hamiltonian dynamical systems obeying Hamilton's equations describe the evolutions of physical systems,[8–10,18] while the thermostatted dynamical systems are often used to describe the driven systems or the systems in contact with external fields, the systems connected to reservoirs or the mechanical pistons or particle reservoirs, as well as the constrained systems, and the systems away from equilibrium.[19] Recently, these studies related to thermostatted systems are focused on the investigation of their ergodicity and topology. Tapias *et al.* proposed a logistic thermostat that is a variant of the Nosé–Hoover oscillator and numerically studied the ergodicity of the system using four tests.[20] Then, Sprott discussed the ergodicity of several one-dimensional oscillators with a signum thermostat based on the logistic thermostat, including a signum thermostatted linear oscillator, a signum thermostatted nonlinear oscillator, a signum thermostatted Duffing oscillator, a signum thermostatted pendulum, and a signum thermostatted square-well oscillator.[21] As for the topological structure, Cang *et al.* proposed an effective method to construct volume-conservative thermostatted systems by modifying the Hamiltonian energy function of a thermostatted system like the Sprott-A system.[22] Based on the method of Ref. [22], several interesting thermostatted systems with different topological structures were found.[23]

In chaos-based applications, pursuing higher-ranking security of cryptosystem needs the chaotic systems with more complicated topological structures. So far, multiple types of topological structure of dissipative chaotic flows have been well studied by many researchers in the field of nonlinear science, such as multi-scroll chaos,[24–26] multi-wing chaos,[27,28] multi-torus chaos,[29] and some new types of chaotic attractors with special topological structures.[30–33] Among these dissipative chaotic systems with complicated topological structure, coexisting attractors only depending on

†Corresponding author. E-mail: sj.cang@gmail.com
© 2022 Chinese Physical Society and IOP Publishing Ltd

initial conditions are one of the hot research areas in the study of special chaotic systems. The coexisting dynamics have also been found in conservative systems, but the coexisting dynamics in Hamiltonian or thermostatted systems differ from the dissipative cases due to the energy/volume conservation of such systems. Although there is a common phenomenon that the invariant tori and conservative chaotic flows, as well as multiple periodic orbits coexist in conservative systems, little attention has been paid to the nonlinear dynamic characteristics of invariant tori and conservative chaotic flows. Similar to the multi-scroll and multi-wing chaotic attractor in dissipative systems, chaotic flows generated from conservative systems can manifest multiple clusters. The Sprott-A system,[34,35] a typical 3D thermostatted system, can produce volume-conservative chaotic flows with one single cluster for the given parameters and initial conditions. To find more complicated thermostatted system, Cang *et al.* proposed a 3D thermostatted system with eight-cluster volume-conservative chaotic flows and separated invariant tori.[36] However, that work only presented numerical investigation and found some amazing dynamical behaviors. It is necessary to theoretically analyze the dynamic characteristics and find why the system can generate complicated conservative flows. In this paper, we mainly concentrate on the nonlinear dynamic analysis and numerical investigation of the system including the geometry of its Hamiltonian, curve axes, as well as multiple equilibria and their stabilities, and the mixture of chaotic seas and islands of invariant tori are numerically investigated for different initial conditions.

The rest of this paper is divided into seven sections as follows. In Section 2, we investigate the structure of the thermostatted system based on the formalism of the generalized Hamiltonian system. In Section 3, we perform the geometrical analysis of the Hamiltonian of the system including isosurfaces for different initial conditions and the local centers. In Section 4, the equilibria of the system and their stabilities are discussed based on two cases. The local curve axes of invariant tori and one eight-cluster conservative flow are explored in Section 5. Furthermore, in Section 6 we demonstrate the mixture of chaotic seas and islands of invariant tori of the thermostatted system. Finally, some conclusions are drawn in Section 7.

2. System model

The thermostatted system with eight-cluster conservative chaotic flows can be described by three first-order ordinary differential equations as follows:[36]

$$\begin{aligned}\dot{x} &= y\left(y^2-a^2\right)+z\left(z^2-a^2\right),\\ \dot{y} &= -x\left(x^2-a^2\right)+yz\left(z^2-a^2\right),\\ \dot{z} &= -x\left(x^2-a^2\right)-y^2\left(y^2-a^2\right)+k,\end{aligned} \tag{1}$$

where x, y and z denote the state variables; $a\in\mathbb{R}$ is the parameter; and $k\geq 0$ represents the external excitation. Due to the existence of k, the system (1) has no scalar function (Hamiltonian) satisfying the Hamilton equation, thus the system (1) is not a Hamiltonian system. However, the system (1) meets the description of the thermostatted system.[19] When $a=2$ and $k=1$, the coexistence of separated invariant tori and eight-cluster conservative chaotic flows appears in the thermostatted system for different initial conditions. At first glance, the system (1) is more complicated than the classic chaotic systems, such as the Lorenz system,[37] Chua's circuit equation,[1] and Duffing oscillator,[38] because there are seven nonlinear terms yz, y^2, x^3, y^3, z^3, yz^3 and y^4, and three linear terms x, y and z, and one constant term k. However, the system (1) can be converted into the following matrix differential equation:

$$\begin{pmatrix}\dot{x}\\ \dot{y}\\ \dot{z}\end{pmatrix}=\begin{pmatrix}0 & 1 & 1\\ -1 & 0 & y\\ -1 & -y & 0\end{pmatrix}\begin{pmatrix}x\left(x^2-a^2\right)\\ y\left(y^2-a^2\right)\\ z\left(z^2-a^2\right)\end{pmatrix}+\begin{pmatrix}0\\ 0\\ k\end{pmatrix}, \tag{2}$$

based on the formalism of the generalized Hamiltonian system.[39] If we let $X=(x,y,z)^{\mathrm{T}}$, the interconnection conservation matrix is

$$J(X)=\begin{pmatrix}0 & 1 & 1\\ -1 & 0 & y\\ -1 & -y & 0\end{pmatrix};$$

the gradient of $H(X)$ is

$$\nabla H(X)=(f_1(x),f_2(y),f_3(z))^{\mathrm{T}},$$

where

$$f_1(x)=x\left(x^2-a^2\right),\ f_2(y)=y\left(y^2-a^2\right),\ f_3(z)=z\left(z^2-a^2\right),$$

and the external excitation $u=(0,0,k)^{\mathrm{T}}$. Numerical results have shown that there exist invariant tori and one eight-cluster conservative chaotic flows.[36] It is well-known that improving the complication of topological structure of chaotic flows can improve the performance of chaos-based encryption algorithms. Recently, many scholars have focused on the studies of the conservative-chaos-based information encryption technologies and achieved promising results.[40,41] In Refs. [40,41], the topological structures of the conservative chaotic flows, which have been used by different information encryption technologies, are pretty simple. However, the system (1) can generate eight-cluster conservative chaotic flows, thus the system has greater potential for information encryption.

For such dynamical behaviors, the isosurface of $H(x)$ determines the whole topological structure, the number of clusters relies on the local centers of $H(X)$, the local curve axes of clusters are subject to $J(X)\nabla H(X)$, and the external excitation $g(X)u$ destroys the motion of the system (1) on the isosurfaces of $H(X)$ and leads to the emergence of invariant tori and conservative chaos. The mechanism of the above characteristics will be investigated in following sections.

3. Geometry of $H(X)$

3.1. Isosurfaces

According to $\nabla H(X) = (f_1(x), f_2(y), f_3(z))^{\mathrm{T}}$, we have a Hamiltonian as follows:

$$\begin{aligned} H(X) &= \int f_1(x)\mathrm{d}x + \int f_2(y)\mathrm{d}y + \int f_3(z)\mathrm{d}z \\ &= G(X) - \frac{3}{4}a^4, \end{aligned} \tag{3}$$

where

$$G(X) = \frac{(x^2-a^2)^2}{4} + \frac{(y^2-a^2)^2}{4} + \frac{(z^2-a^2)^2}{4}. \tag{4}$$

Obviously, $G(X) \geq 0$ denotes a closed surface that is compact and without boundary. When $k = 0$, the Hamiltonian (3) is the first integral of the system (1). For different $G(X)$, the isosurfaces manifest various shapes, which can be summarized as the seven cases in Table 1.

Table 1. $G(X)$ and its different shapes.

Cases	$G(X)$	Shapes	Figures
1	$=0$	eight separated points	Fig. 1(a)
2	$\in (0, \frac{1}{4}a^4)$	eight separated surfaces	Fig. 1(b)
3	$=\frac{1}{4}a^4$	critical case between eight separated surfaces and one hollowed-out surface	Fig. 1(c)
4	$\in (\frac{1}{4}a^4, \frac{1}{2}a^4)$	one hollowed-out surface	Fig. 1(d)
5	$=\frac{1}{2}a^4$	critical case between one hollowed-out surface and one surface with one inner cavity	Fig. 1(e)
6	$\in (\frac{1}{2}a^4, \frac{3}{4}a^4)$	one surface with one inner cavity	Fig. 1(f)
7	$\in [\frac{3}{4}a^4, +\infty)$	one surface without inner cavity	Fig. 1(g)

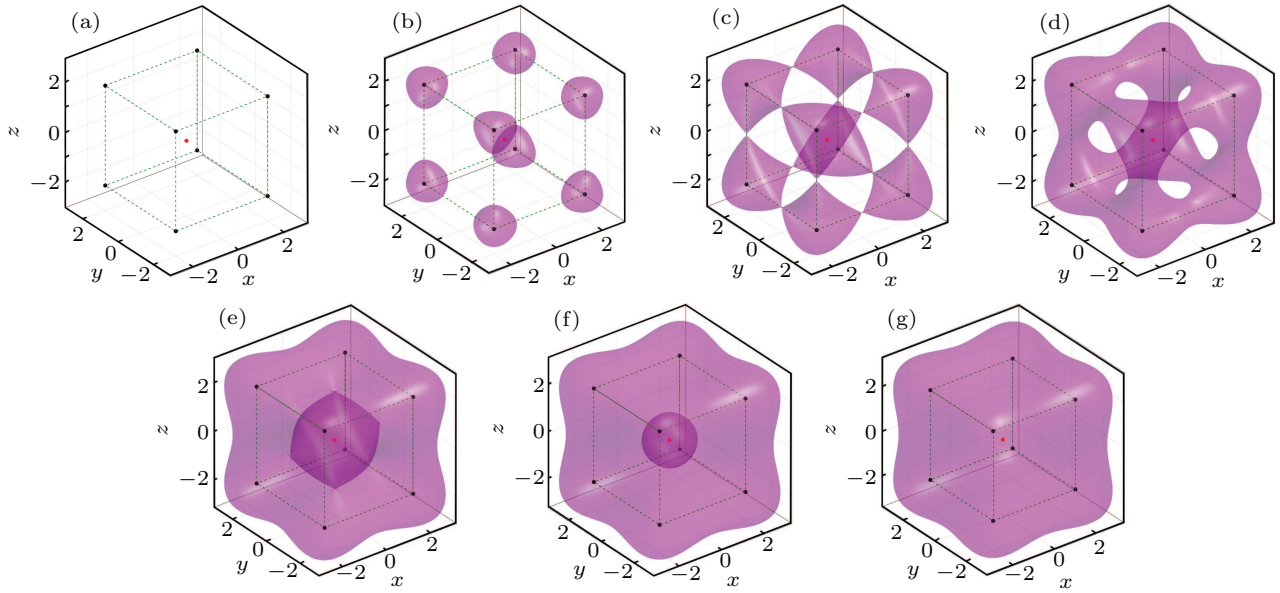


Fig. 1. Cases of the 3D view of the isosurfaces (invariants) of $H(X)$ with the increasing $G(X_0)$ for $a = 2$: (a) eight separated points, (b) eight separated surfaces, (c) critical case between eight separated surfaces and one hollowed-out surface, (d) one hollowed-out surface, (e) critical case between one hollowed-out surface and one surface with one inner cavity, (f) one surface with one inner cavity, (g) one surface without inner cavity.

When $a = 2$, the isosurfaces of these seven cases can be exhibited in Fig. 1. Let $X_0 = (x_0, y_0, z_0)^{\mathrm{T}}$ be the initial conditions of the system (1), then substituting X_0 into Eq. (4) yields an isosurface $G(X_0)$. With $k = 0$, the trajectory starting from X_0, denoted by $\phi(X_0, X, t)$, always runs on $G(X_0)$ because the conserved quantity of Eq. (2) does not vary over time, i.e., $\mathrm{d}H(X)/\mathrm{d}t = 0$.

3.2. Local centers of isosurfaces

According to Eqs. (3) and (4), $H(X)$ reaches the minimum $-\frac{3a^4}{4}$ at $x = \pm a$, $y = \pm a$ and $z = \pm a$. In this case, the isosurfaces of $G(X)$ are degenerated into eight isolated points, as shown in Fig. 1(a). With the increment of $G(X)$, these minimum points remain unchanged, as shown in Figs. 1(b)–1(g), which means that $C_{1,2,\cdots,8} = \{(x,y,z) \in \mathbb{R}^3 | x = \pm a, y = \pm a, z = \pm a\}$ are the eight local centers of $H(X)$. However, not all $H(X)$ can be expressed as the sum of squares by the method of completing the square. For a more general $H(X)$, its local centers can be determined by its Hessian matrix at these points satisfying $\nabla H(X) = 0$. If $\nabla H(X) = 0$, twenty-seven solutions can be obtained as follows:

$$\begin{aligned} & C_{1,2,\cdots,8} \cup C_{9,10,11,12} \cup C_{13,14,15,16} \cup C_{17,18} \\ & \cup C_{19,20,21,22} \cup C_{23,24} \cup C_{25,26} \cup C_0 \\ = \ & \{(\pm a, \pm a, \pm a), (\pm a, 0, \pm a), (\pm a, \pm a, 0), (\pm a, 0, 0), \\ & (0, \pm a, \pm a), (0, 0, \pm a), (0, \pm a, 0), (0, 0, 0)\}. \end{aligned} \tag{5}$$

Among these stationary points of $H(X)$, some points are the local minimum points and the others are the inflection points. Obviously, $C_{1,2,\cdots,8}$ are just parts of Eq. (5), but ruling out other solutions of $\nabla H(X)=0$ needs to use the Hessian matrix at each solution of $\nabla H(X)=0$. The Hessian matrix of $H(X)$ is

$$Hs=\begin{pmatrix}3x^2-a^2 & 0 & 0\\ 0 & 3y^2-a^2 & 0\\ 0 & 0 & 3z^2-a^2\end{pmatrix}. \tag{6}$$

If Eq. (6) is positive definite, we have

$$x,y,z\in\left(-\infty,-\frac{\sqrt{3}a}{3}\right)\cup\left(\frac{\sqrt{3}a}{3},+\infty\right). \tag{7}$$

Let $Hs|_{C_n}$ $(n=0,1,\ldots,26)$ be the nth solution of $\nabla H(X)=0$, then substituting the solution C_n $(n=0,1,\ldots,26)$ into Eq. (6), we can find that $Hs|_{C_n(n=1,2,\ldots,8)}$ is positive definite, which means that $C_{1,2,\ldots,8}$ are the local minimum points of $H(X)$. When $G(X)$ gradually increases, the isosurface denoted by $G(X)$ swells up from $C_{1,2,\ldots,8}$, as shown in Fig. 1. Thus, $C_{1,2,\ldots,8}$ are the local centers of $G(X)$, while the others are not, which agrees well with the results obtained by the method of completing the square.

For different $G(X_0)$, the solutions of $\nabla H(X)=0$ remain the same. When $G(X_0)$ equals 3.7959 and 4.4561, the solutions of $\nabla H(X)=0$ are shown in Figs. 2 and 3, respectively, in which the green dots denote the inflection points of $H(X)$, while the black ones represent the local centers of $H(X)$, which are exactly distributed in the eight corners of a single crystal lattice. Investigating the local centers of $H(X)$ is helpful for locating invariant tori and cluster-shaped conservative chaotic flows.

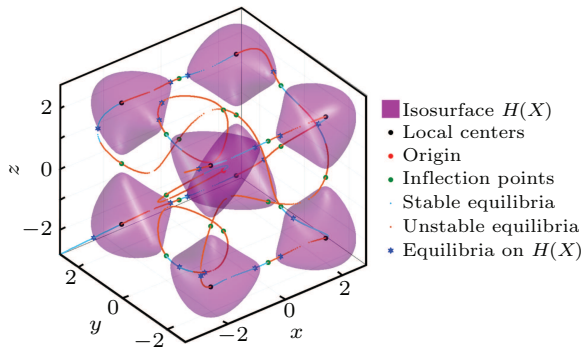


Fig. 2. For $a=2$, the superposition of the isosurface $H(X)$ with $G(X_0)=3.7969$ (purple surface), the local centers (black solid circles), the inflection points (green solid circles), the curves of stable equilibria (light blue curves) and unstable equilibria (orange curves) of the system (1) with $k=0$, and the equilibria on $H(X)$ (blue hexagrams) in 3D phase space.

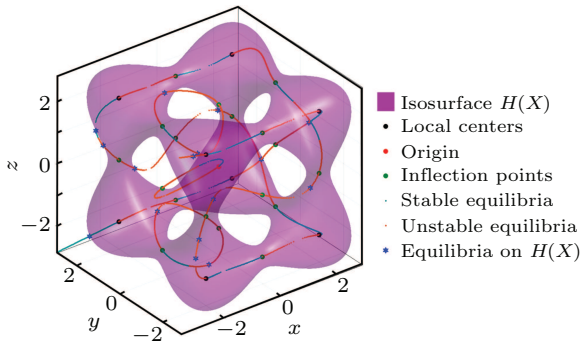


Fig. 3. For $a=2$, the superposition of the isosurface $H(X)$ with $G(X_0)=4.4561$ (purple surface), the local centers (black solid circles), the inflection points (green solid circles), the curves of stable equilibria (light blue curves) and unstable equilibria (orange curves) of the system (1) with $k=0$, and the equilibria on $H(X)$ (blue hexagrams) in 3D phase space.

4. Equilibria and stability

For the nonzero parameter a, the system (1) has countless equilibria for $k=0$ and no equilibrium for $k\neq 0$. Thus, the system (1) is a chameleon system.[42] For the case of $k=0$, the equilibria of Eq. (1) can be obtained by $\dot{x}=0$, $\dot{y}=0$ and $\dot{z}=0$, and one obtains the equilibria set

$$\begin{aligned}E_r=\{&(x_e,y_e,z_e)\in\mathbb{R}^3|x_e\left(x_e^2-a^2\right)=rh(r),\\ &y_e=r,\ z_e\left(z_e^2-a^2\right)=h(r)\},\end{aligned} \tag{8}$$

where the parameter r denotes any real number and $h(r)=-r\left(r^2-a^2\right)$. When r varies, the set E_r denotes multiple curves of equilibria. For example, when $r\in[-3,3]$, it can be found there are five curves, as shown in Figs. 2 and 3.

For dynamical systems with equilibria, the local dynamical behaviors near equilibria can be determined by their corresponding Jacobian matrix. For the system (1), whether k equals zero or not, its Jacobian matrix $J_m(X)$ can be obtained as

$$\begin{aligned}J_m(X)&=\frac{\partial(\dot{x},\dot{y},\dot{z})}{\partial(x,y,z)}\\ &=\begin{pmatrix}0 & 3y^2-a^2 & 3z^2-a^2\\ a^2-3x^2 & z^3-a^2z & 3yz^2-a^2y\\ a^2-3x^2 & 2a^2y-4y^3 & 0\end{pmatrix}.\end{aligned} \tag{9}$$

As the solutions of $\nabla H(X)=0$ are also the solutions of $J(X)\nabla H(X)=0$, the local centers and inflection points are in the curves of equilibria E_r. Substituting C_n $(n=0,1,\ldots,26)$ into Eq. (9), the corresponding eigenvalues show that $C_{13,14,\ldots,18}$ and $C_{23,24,\ldots,26}$ are saddle equilibria, while the others are nonhyperbolic equilibria. When $r\in[-3,3]$, the stability of all equilibria represented by Eq. (8) can be depicted by different color curves in Figs. 2 and 3. The countless light blue points denote the stable equilibria, while the orange points represent the unstable equilibria. Note that the stabilities of all equilibria are not affected by the initial conditions.

Table 2. Equilibria and their stabilities of the system (1) with $k = 0$ on $G(X_0) = 3.7969$.

Equilibria				Eigenvalues (λ_1, λ_2)		Types of equilibria
S_i	x_e	y_e	z_e			
S_1	–2.6864	–2.3570	2.3570	1.8331–38.0068i	1.8331+38.0068i	Unstable focus
S_2	–2.5918	–2.3072	–1.2409	1.5264-15.6476i	1.5264+15.6476i	Unstable focus
S_3	0.3641	–2.0798	–1.9093	0.3385-14.8883i	0.3385+14.8883i	Unstable focus
S_4	0.3599	–2.0790	2.0790	0.3350-17.1793i	0.3350+17.1793i	Unstable focus
S_5	–0.3756	–1.8966	–2.0894	–0.3819-12.3315i	–0.3819+12.3315i	Stable focus
S_6	–0.3827	–1.8945	1.8945	–0.3892-10.2981i	–0.3892+10.2981i	Stable focus
S_6	2.3621	–1.2169	1.2169	–1.5328-2.7503i	–1.5328+2.7503i	Stable focus
S_8	–1.4084	–0.9607	–2.2991	3.8700	–6.8265	Saddle
S_9	–1.8945	–0.4528	–2.1876	–0.8591–5.5854i	–0.8591+5.5854i	Stable focus
S_{10}	2.0879	–0.4441	–2.1847	–0.8445–6.8808i	–0.8445+6.8808i	Stable focus
S_{11}	2.0879	0.4441	2.1847	0.8445-6.8808i	0.8445+6.8808i	Unstable focus
S_{12}	–1.8945	0.4528	2.1876	0.8591-5.5854i	0.8591+5.5854i	Unstable focus
S_{13}	–1.4084	0.9607	2.2991	6.8265	–3.8700	Saddle
S_{14}	2.3621	1.2169	–1.2169	1.5328-2.7503i	1.5328+2.7503i	Unstable focus
S_{15}	–0.3827	1.8945	–1.8945	0.3892-10.2981i	0.3892+10.2981i	Unstable focus
S_{16}	–0.3756	1.8966	2.0894	0.3819-12.3315i	0.3819+12.3315i	Unstable focus
S_{17}	0.3599	2.0790	–2.0790	–0.3350-17.1793i	–0.3350+17.1793i	Stable focus
S_{18}	0.3641	2.0798	1.9093	–0.3385-14.8883i	–0.3385+14.8883i	Stable focus
S_{19}	–2.5918	2.3072	1.2409	–1.5264-15.6476i	–1.5264+15.6476i	Stable focus
S_{20}	–2.6864	2.3570	–2.3570	–1.8331-38.0068i	–1.8331+38.0068i	Stable focus

Table 3. Equilibria and their stabilities of the system (1) with $k = 0$ on $G(X_0) = 4.4561$.

Equilibria				Eigenvalues (λ_1, λ_2)		Types of equilibria
S_i	x_e	y_e	z_e			
S_1	–2.7366	–2.3834	2.3834	2.0028–39.6028i	2.0028+39.6028i	Unstable focus
S_2	–2.5840	–2.3031	–1.0035	1.5017–10.2174i	1.5017+10.2174i	Unstable focus
S_3	–2.4006	–2.2066	–0.5132	10.0133	–8.0956	Saddle
S_4	1.5883	–2.1258	–0.2815	12.8376	–11.7339	Saddle
S_5	–1.5875	–1.8124	0.3333	6.7363	–8.0325	Saddle
S_6	2.3315	–1.0921	1.0921	–4.8663	1.8004	Saddle
S_6	–1.1357	–1.0197	–2.3043	5.6576	–8.6758	Saddle
S_8	–1.4648	–0.9311	1.3647	1.3531	–4.2703	Saddle
S_9	–1.4648	0.9311	–1.3647	4.2703	–1.3531	Saddle
S_{10}	–1.1357	1.0197	2.3043	8.6758	–5.6576	Saddle
S_{11}	2.3315	1.0921	–1.0921	–1.8004	4.8663	Saddle
S_{12}	–1.5875	1.8124	–0.3333	8.0325	–6.7363	Saddle
S_{13}	1.5883	2.1258	0.2815	11.7339	–12.8376	Saddle
S_{14}	–2.4006	2.2066	0.5132	8.0956	–10.0133	Saddle
S_{15}	–2.5840	2.3031	1.0035	–1.5017–10.2174i	–1.5017+10.2174i	Stable focus
S_{16}	–2.7366	2.3834	–2.3834	–2.0028–39.6028i	–2.0028+39.6028i	Stable focus

As mentioned above, for the given initial conditions, there are isosurfaces with different shapes when $k = 0$. According to the curves of equilibria E_r in Figs. 2 and 3, we clearly see that there are some intersections of $G(X_0)$ and E_r. The numbers of the intersections depend on $G(X_0)$. When $G(X_0) = 3.7969$, eight separated surfaces appear, however, when $G(X_0) = 4.4561$, the geometry of $H(X)$ manifests one hollowed-out surface. For these two cases, their intersections of $G(X_0)$ and E_r are listed in Tables 2 and 3, respectively.

From Table 2, we can see that there are twenty intersections of $G(X_0)$ and E_r, which means that the system (1) has twenty equilibria for $k = 0$ on the isosurface $G(X_0) = 3.7969$. Among them, there are nine unstable foci, nine stable foci and two saddles. The trajectory starting from a point on $G(X_0)$ converges to one of the nine stable foci. However, when $G(X_0) = 4.4561$, the eight separated surfaces inflate and merge into one hollowed-out surface, which leads to the change of the intersections of $G(X_0)$ and E_r. In this case, Table 3 records sixteen intersections of $G(X_0)$ and E_r, which include two stable foci, two unstable foci, and twelve saddles. All initial conditions on $G(X_0)$ result in the generated flows approaching one of the two stable foci. In Figs. 2 and 3, the blue hexagrams denote the equilibria for the given $G(X_0)$.

Hereto, we have analyzed the geometry of $H(X)$ and the equilibria of the system (1) as well as their local stabilities when $k = 0$. In the following section, we focus on the global dynamical behaviors of the system (1) including invariant tori and conservative chaos when $k = 1$.

5. Curve axes of $\phi(X,X_0,t)$

As for cluster-shaped objects, there is always one or more invisible line or curve axis in it, such as a ball of wool and the field distribution in a dipole magnet. In the cluster-shaped conservative invariant tori and chaotic flows, there may be one or more invisible line or curve axes. For the system (1), we define the trajectory emanating from the initial condition X_0 as $\phi(X,X_0,t)$. For $k=0$, $\phi(X,X_0,t)$ is always on $G(X_0)$, while for $k\neq 0$, $\phi(X,X_0,t)$ forms invariant tori and eight-cluster conservative chaotic flows, which have been numerically explored.[39]

As mentioned in Section 3.1, there exists a first integral $H(X)$ (Hamiltonian energy function) when $k=0$. In this case, the system (1) is energy-conservative. However, when $k\neq 0$, no Hamiltonian satisfies $\mathrm{d}H(X)/\mathrm{d}t=0$ because there exists energy exchange between Eq. (1) and external environment caused by k. To simplify system analysis, we can define the external system exchanging energy as

$$\dot{v}=-kf_3(z), \tag{10}$$

where v is an augmented variable belonging to the external system. Combining Eqs. (1) and (10) yields

$$\begin{aligned}\dot{x}&=f_2(y)+f_3(z),\\ \dot{y}&=-f_1(x)+yf_3(z),\\ \dot{z}&=-f_1(x)+yf_2(y)+k,\\ \dot{v}&=-kf_3(z),\end{aligned} \tag{11}$$

and its integrated Hamiltonian $H'(X)$ is

$$H'(X)=H(X)-k\int z(z^2-a^2)\mathrm{d}t. \tag{12}$$

Obviously, the term k is the only route realizing the energy exchange between Eqs. (1) and (10). For $k=0$, $H'(X)$ is one first integral of Eq. (1), while for $k\neq 0$, $H'(X)$ is one first integral of Eq. (11). If $\varphi(X,X_0,t)$ denotes the trajectory generated by Eq. (11), $\varphi(X,X_0,t)$ should run on the hypersurface $H'(X_0)$ in (x,y,z,v) space. Since the system (1) is the subsystem of the system (11), $\phi(X,X_0,t)$ is the projection of $\varphi(X,X_0,t)$ in (x,y,z) space.

Without the external excitation k, $\phi(X,X_0,t)$ approaches one of the stable equilibria (intersections of E_r and $G(X)$). However, when the external excitation is introduced into Eq. (1), $H(X)$ and E_r will be destroyed. Here, $\phi(X,X_0,t)$ running on $G(X)$ approaches or keeps away from the neighborhood of E_r. In a small enough area near E_r, we can reach the following approximate solution of Eq. (1):

$$x(t)\approx x_e^s,\ \ y(t)\approx y_e^s,\ \ z(t)\approx z_e^s+kt, \tag{13}$$

where the superscript s denotes the stable equilibria in E_r when $k=0$. E_r is not an isolated point but multiple curves of equilibria, and $\phi(X,X_0,t)$ not only converges to or keeps away from E_r but also moves with E_r. This dynamical behavior differs from that of the case of an isolated equilibrium. If E_r is stable, $\phi(X,X_0,t)$ converges to E_r; conversely, $\phi(X,X_0,t)$ is away from E_r. It should be noted that k can be regarded as the speed of the local movement near E_r.

For 3D thermostatted systems without external excitation, chaos does not appear due to the existence of the invariant. When the external periodic or fixed signal is introduced into the system, the conservative dynamics including conservative chaos and invariant tori may appear. Although the local dynamical behaviors can be determined by the Jacobian matrix of Eq. (1), the dynamical behaviors near E_r can be imaged even though $k\neq 0$. As long as $k\neq 0$, the local dynamical behaviors near E_r cannot be sustained over time because $z(t)\approx z_e^s+kt$. For $a=2$, the system (1) undergoes invariant tori and volume-conservative chaos for different X_0.

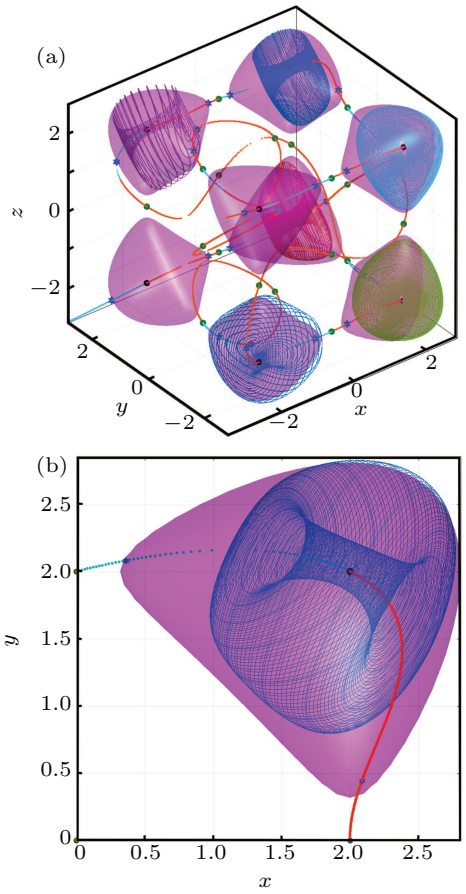


Fig. 4. Invariant tori surrounding six isolated isosurfaces where different colors of tori denote the flows generated by the system (1) under different initial conditions with the corresponding curve axes: (a) 3D view of the six tori connected by two curve axes, (b) 2D magnification of the tori generated by the system (1) (blue) with $X_0=(\frac{5}{2},\frac{5}{2},\frac{5}{2})$, local center and curve axis.

If $(\frac{5}{2},\pm\frac{5}{2},\pm\frac{5}{2})$, $(-\frac{5}{2},\frac{5}{2},\frac{5}{2})$ and $(-\frac{5}{2},-\frac{5}{2},-\frac{5}{2})$ are selected as the six groups of initial conditions on $G(X_0)$, $\phi(X,X_0,t)$ of Eq. (1) will form six separated cluster-shaped invariant tori surrounded by $G(X_0)$, which are plotted by different color curves in Fig. 4(a). Figure 4(a) shows the superposition of the local centers $C_{1,2,\ldots,8}$, six cluster-shaped invariant tori

$\phi(X,X_0,t)$, curves of equilibria E_r and isosurface $G(X_0) = 3.7969$. It can be found that these cluster-shaped invariant tori are chained together by the curves of equilibria E_r. For $\phi(X,X_0,t)$ with $X_0 = (\frac{5}{2},\frac{5}{2},\frac{5}{2})$, the details on the (x,y) plane $(z=2)$ can be seen in Fig. 4(b). Clearly, there is a curve axis through the local center (2, 2, 2) and $\phi(X,X_0,t)$.

If $X_0 = (\frac{5}{4},\frac{5}{4},-\frac{5}{4})$, an eight-cluster conservative chaotic flow will appear, as shown in Fig. 5. In this case, its three Lyapunov exponents can be obtained as $(LE_1,LE_2,LE_3) = (0.1448,0,-0.1448)$. The largest Lyapunov exponent LE_1 is greater than zero, and the sum of all Lyapunov exponents is zero, indicating that the system (1) is volume-conservative and chaotic. From Fig. 5(a), the superposition of $C_{1,2,\ldots,8}$, $\phi(X,X_0,t)$, E_r and $G(X_0) = 4.4561$ shows that the cluster-shaped chaotic flows are chained together by E_r. Similarly, based on the details of $\phi(X,X_0,t)$ projected on the (x,y) plane in Fig. 5(b), we can also find that there is a curve axis through the local center $(-2, 2, -2)$ and $\phi(X,X_0,t)$.

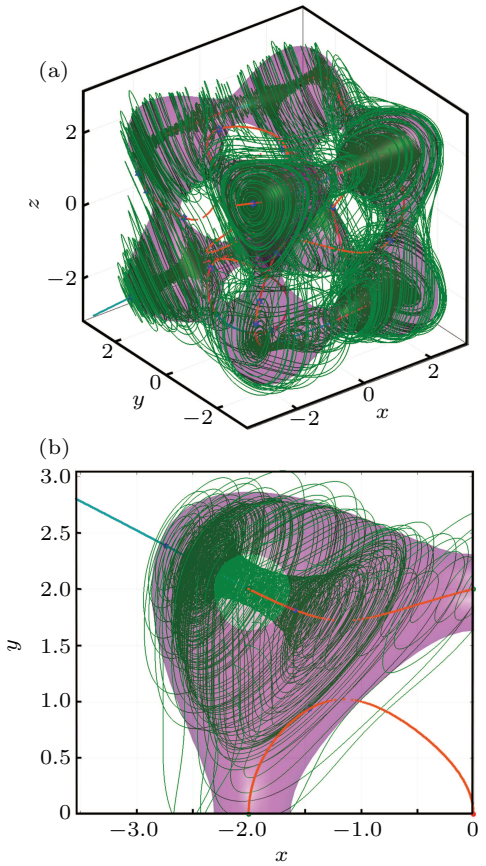


Fig. 5. Chaos surrounding the one hollowed-out surface where the green trajectories denote the volume-conservative chaotic flows generated from Eq. (2) with $X_0 = (\frac{5}{4},\frac{5}{4},-\frac{5}{4})$ and the corresponding curve axes: (a) 3D view of the eight-cluster volume-conservative chaotic flows, (b) 2D magnification of the chaotic flows of one of clusters, local center and curve axes.

Based on the numerical analysis of the two cases, the curve axes of $\phi(X,X_0,t)$ have three significant characteristics as follows:

(1) The curve axes consist in the curves of equilibria E_r of the thermostatted system with zero external excitation.

(2) Any one of the curve axes must have a center locating in the curves of equilibria E_r.

(3) With the center as a boundary, the equilibria on one side of the curve axes are stable (curves colored light blue) and the equilibria on another side are unstable (curves colored orange), as shown in Figs. 4(b) and 5(b).

According to Figs. 2 and 3, there are eight curve axes in E_r, and the system (1) may have eight invariant tori or one eight-cluster conservative chaotic flow under different initial conditions on $G(X)$, which were verified by the numerical results in Figs. 4 and 5.

6. Chaotic seas and stable islands

Dynamical systems can be understood from the motions of their state points on the Poincaré sections. The Poincaré return maps of Hamiltonian and thermostatted chaotic systems consist of chaotic seas and islands of invariant tori. Generally, there are chains of islands around each of the critical invariant tori, and chaotic seas remain in close contact with the critical invariant tori encircling countless hierarchical islands of invariant tori.[43] For the system (1) with $a = 2$ and $k = 1$, the Poincaré return map on the surface of the section $x = 2.1$ is plotted in Fig. 6, which shows a mixture of chaotic seas and islands of invariant tori. It can be found from Fig. 6 that there are four groups of chains of islands of invariant tori, i.e., G1, G2, G3 and G4, and all of them contain five families of invariant tori. Moreover, we can see that the chaotic motion is stuck by the critical invariant tori and stays there for a long time since the local expansion rate of nearby stable invariant tori is approximately zero. The stickiness of chaotic motion to the islands of invariant tori occurs repeatedly and intermittently, and produces a long-time correlation of chaotic motion. Also, we can clearly observe that the return points on the Poincaré section at $x = 2.1$ form two white stripes, which means that there are no return points distributed in the stripes. The stripes rely on the curves of equilibria E_r. According to the equilibria set (8), eliminating the state variable x yields

$$(y_e + z_e)\left(y_e^2 - y_e z_e + z_e^2 - a^2\right) = 0. \tag{14}$$

Then,

$$z_e = -y_e, \quad y_e^2 - y_e z_e + z_e^2 = a^2, \tag{15}$$

which indicates that the curves of equilibria E_r projected on the (y,z) plane manifest one line through the origin, and one ellipse centered at the origin. If we plot the line and the ellipse on the Poincaré section at $x = 2.1$, we can find that the line and the ellipse are exactly filled in the two white stripes, as shown in Fig. 7.

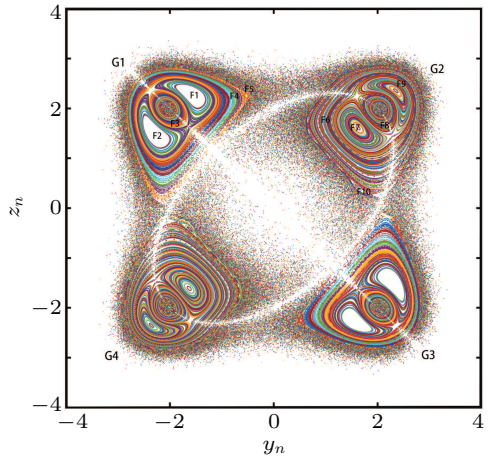


Fig. 6. Poincaré return map to the surface of the section $x = 2.1$. The family of invariant tori F4 (or F6) in G1 (or G2) encircles F1, F2 and F3 (or F7, F8 and F9), while F5 and F10 are isolated. Here, the Poincaré section $x = 2.1$ is chosen based on some simulations since this Poincaré section is representative and can show more information related to stable islands.

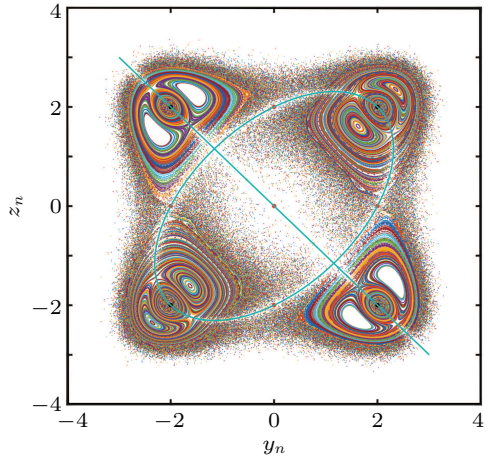


Fig. 7. Superposition of the Poincaré return map and the projected curve axes E_r on the (y_n, z_n) plane at $x = 2.1$.

7. Conclusion

In literature, there have been few studies on the dynamic characteristics analysis of conservative flows from thermostatted systems. Based on one complicated thermostatted system, we systematically investigate its multiple equilibria and curve axes of cluster-shaped invariant tori and one eight-cluster conservative chaotic flow. Moreover, several numerical techniques have been used to show that the geometry of the Hamiltonian including different shapes of isosurface and the local centers is explored for different initial conditions. Without external excitation, there exist curves of equilibria in the system in which some segments are stable and others are unstable, and the intersections of curves of equilibria and isosurface determine the dynamical behaviors on the isosurface. However, if there is an external excitation, the curves of equilibria of the system will disappear, and the disappeared curves of equilibria become the curve axes of the invariant tori and eight-cluster conservative chaotic flows. Moreover, the three significant characteristics of curve axes are summarized based on the numerical results. Furthermore, we investigate the chaotic seas and islands of invariant tori for the thermostatted system with given parameters, which shows that the chaotic motion is strongly trapped in the vicinity of each critical invariant tori.

However, there is still one open research question. For given initial conditions (initial energy), there exists energy exchange between the thermostatted system and the external environment. When the energy exchange causes the system to move only near one of curve axes, an invariant torus appears. If the system moves and passes through more than one curve axis, multiple cluster-shaped conservative chaos will arise. Why do different initial conditions lead to different dynamics of the energy exchange process? Further studies are necessary to find a solution to this question.

Acknowledgements

Project supported by the National Natural Science Foundation of China (Grant Nos. 61973175 and 61873186), the South African National Research Foundation (Grant No. 132797), the South African National Research Foundation Incentive (Grant No. 114911), and the South African Eskom Tertiary Education Support Programme.

References

[1] Matsumoto T 1984 *IEEE Trans. Circuits Syst.* **31** 1055
[2] Levien R and Tan S 1993 *Am. J. Phys.* **61** 1038
[3] Xu H Y, Wang G L, Huang L and Lai Y C 2018 *Phys. Rev. Lett.* **120** 124101
[4] Hillebrand M, Kalosakas G, Schwellnus A and Skokos C 2019 *Phys. Rev. E* **99** 022213
[5] Singh J P, Roy B K and Jafari S 2018 *Chaos Soliton. Fract.* **106** 243
[6] Zheng J and Hu H P 2020 *Chin. Phys. B* **29** 090502
[7] Ouannas A, Khennaoui A A, Momani S, Pham V-T and El-Khazali R 2020 *Chin. Phys. B* **29** 050504
[8] Hénon M and Heiles C 1964 *Astron. J.* **69** 73
[9] Lakshmanan M and Sahadevan R 1993 *Phys. Rep.* **224** 1
[10] Esser B and Schanz H 1994 *Chaos Soliton. Fract.* **4** 2067
[11] Sáenz P J, Cristea-Platon T and Bush J W 2018 *Nat. Phys.* **14** 315
[12] Zhang K, Chen W, Bhattacharya M and Meystre P 2010 *Phys. Rev. A* **81** 013802
[13] Barrio R, Blesa F and Serrano S 2010 *Int. J. Bifur. Chaos* **20** 1293
[14] Dong E Z, Li R H, Du S Z 2021 *Chin. Phys. B* **30** 020505
[15] Li S, Cen X and Zhao Y 2017 *Nonlinear Anal.-Real World Appl.* **34** 140
[16] Sabarathinam S and Thamilmaran K 2015 *Chaos Soliton. Fract.* **73** 129
[17] Cang S J, Li Y, Xue W, Wang Z H and Chen Z Q 2020 *Nonlinear Dyn.* **99** 1699
[18] Frahm K M and Shepelyansky D L 2018 *Phys. Rev. E* **98** 032205
[19] Tuckerman M E, Liu Y, Ciccotti G and Martyna G J 2001 *J. Chem. Phys.* **115** 1678
[20] Tapias D, Bravetti D P and Sanders D P 2017 *Comput. Methods Sci. Technol.* **23** 11
[21] Sprott J C 2018 *Comput. Methods Sci. Technol.* **24** 169
[22] Cang S J, Li Y, Kang Z J and Wang Z H 2020 *Chaos* **30** 033103
[23] Cang S J, Li Y, Kang Z J and Wang Z H 2020 *Chaos Soliton. Fract.* **133** 109651
[24] Yuan F, Wang G and Wang X 2016 *Chaos* **26** 073107
[25] Lin Y and Wang C 2016 *Electron. Lett.* **52** 1295
[26] Ding P F, Feng X Y and Wu C M 2020 *Chin. Phys. B* **29** 108202
[27] Zhou L, Wang C and Zhou L 2016 *Nonlinear Dyn.* **85** 2653
[28] Dong E Z, Wang Z, Yu X, Chen Z Q and Wang Z H 2018 *Chin. Phys. B* **27** 010503

[29] Yu S, Lu J and Chen G 2007 *IEEE Trans. Circuits Syst. I* **54** 2087
[30] Letellier C, Gilmore R and Jones T 2007 *Phys. Rev. E* **76** 066204
[31] Letellier C and Aguirre L A 2012 *Phys. Rev. E* **85** 036204
[32] Wang Z L, Cang S J, Wang Z H, Xue W and Chen Z Q 2014 *Abstr. Appl. Anal.* **2014** 495126
[33] Cang S J, Wu A G, Wang Z L, Wang Z H and Chen Z Q 2016 *Nonlinear Dyn.* **83** 1069
[34] Sprott J C 1994 *Phys. Rev. E* **50** R647
[35] Messias M and Reinol A C 2018 *Nonlinear Dyn.* **92** 1287
[36] Cang S J, Li Y and Wang Z H 2018 *Int. J. Bifur. Chaos* **28** 1830044
[37] Lorenz E N 1963 *J. Atmos. Sci.* **20** 130
[38] Guckenheimer J and Holmes P 1983 *Nonlinear oscillations, dynamical systems, and bifurcations of vector fields* (Germany: Springer Science & Business Media) p. 39
[39] Van Der Schaft A and Jeltsema D 2014 *Found. Trends Syst. Control* **1** 173
[40] Zhou M and Wang C 2020 *Signal Process.* **171** 107484
[41] Cang S, Kang Z and Wang Z 2021 *Nonlinear Dyn.* **104** 827
[42] Jafari M A, Mliki E, Akgul A, Pham V T, Kingni S T, Wang X and Jafari S 2017 *Nonlinear Dyn.* **88** 2303
[43] Ishizaki R, Horita T and Mori H 1993 *Prog. Theor. Phys.* **89** 947